



The effect of platinum contact metallization on Cu/Sn bonding

Antti Rautiainen¹ · Glenn Ross¹ · Vesa Vuorinen¹ · Hongqun Dong¹ · Mervi Paulasto-Kröckel¹

Received: 2 March 2018 / Accepted: 12 July 2018 / Published online: 16 July 2018
© Springer Science+Business Media, LLC, part of Springer Nature 2018

Abstract

In this work, formation and evolution of microstructures in CuSn/Pt bonding were investigated after 320 °C reflow process as well as after high temperature storage test at 150 °C. Sputtered thin film platinum on silicon wafer and high purity platinum sheet were applied as contact metallizations for electroplated copper-tin based bonding metallurgy. As bonded microstructure showed PtSn₄ intermetallic compound growth at the Pt/Sn interface, and both Cu₆Sn₅ and Cu₃Sn phases formed at the Cu/Sn interface. Both hexagonal and monoclinic Cu₆Sn₅ were found to coexist after 1000 h high temperature storage test. Platinum was discovered to dissolve into the Cu₆Sn₅ phase during soldering process and form (Cu, Pt)₆Sn₅ intermetallic compound exhibiting hexagonal allotropy. Meanwhile, under annealing, monoclinic Cu₆Sn₅ phase layer without platinum was observed to form between (Cu, Pt)₆Sn₅ grains and tin. Thermodynamic analysis was performed in order to reason the effects of Pt on the phase equilibria and phase stabilities. Results show that platinum has a significant impact on the stability of hexagonal Cu₆Sn₅.

1 Introduction

The continuous growth in performance of electronics is based on enhancing the integration level with the “More-than-Moore” approach [1, 2]. This platform can be applied to functional units such as processor, memory, sensors and actuators by wafer-to-wafer bonding and using through-silicon vias (TSVs). Metal bonding is a promising method for connecting wafers having different types of functions as well as in wafer-level packaging of IC and microelectromechanical systems (MEMS) [3–5]. As interconnect dimensions reduce drastically, the result is that a large fraction of the bond microstructure consists only of intermetallic compounds (IMCs) [3, 6, 7]. At this scale, the interfacial reactions play a significant role in the wafer bonding process as well as under subsequent assembly processes, which finally has direct impact on the bond performance. Thus, understanding the growth of IMCs together with microstructural properties is crucial for designing reliable devices [8–11]. Overall, the selection of materials and processing

conditions will have a major influence on the performance of the advanced devices.

The copper-tin metallurgy is commonly utilized for interconnections due its mature manufacturing processes and experience. It is very suitable solution for several substrates, however, when considering stable contact metallization on the complex MEMS device wafer or integrated circuit (IC) wafer, platinum is a possible candidate as it is CMOS-compatible, does not oxidize and it reacts slower than gold, silver or palladium with liquid tin; yet exhibiting sufficient wetting performance [12, 13]. Platinum also dissolves into liquid tin slower than nickel [12], the typical diffusion barrier utilized in Cu/Sn soldering, thus platinum could be utilized without additional buffer layer. As a result, process integration is streamlined when several features required from the contact metallization can be combined into one layer. In addition, platinum is biocompatible, which makes it extremely suitable for biomedical applications such as implantable devices, sensing electrodes, neuromodulators and microfluidic chips [14–17].

However, there is a limited amount of experimental data in the literature about interfacial reactions in CuSn/Pt system having μ -bump dimensions (< 10 μ m thick metal layers). Wang et al. studied the cross-interaction between copper and platinum sides having 150 μ m thick tin solder in between bulk substrates, and reflowed the stack different periods from 10 s up to 1 h [18]. Solubility of the platinum

✉ Antti Rautiainen
Antti.rautiainen@aalto.fi

¹ Department of Electrical Engineering and Automation, School of Electrical Engineering, Aalto University, PO Box 13500, FI 00076 Aalto, Finland

into the opposite side Cu–Sn intermetallic compounds was not observed, which is contradictory to results presented by Amagai [19] who reported dissolution of platinum into the Cu_6Sn_5 phase. On the other hand, in several publications, it has been shown that third element can stabilize the high temperature hexagonal (η) crystal structure of the Cu_6Sn_5 phase by preventing the polymorphic transformation to monoclinic (η'). For example, the effect of Ni [20–31], Au [20, 27, 32], Co [27, 29, 30, 33, 34], Fe [28, 29, 33, 34], Pt [19, 27], Pd [35, 36], Zn [20, 32] and In [32, 37], to the Cu_6Sn_5 phase has been investigated extensively. Especially nickel has exhibited interesting results regarding the Cu–Sn interfacial microstructure and particularly the Cu_6Sn_5 phase [26, 28, 29, 31]. It has been confirmed in several publications [25, 26, 32, 38, 39] that as little as 1 at% of nickel in the Cu_6Sn_5 phase stabilizes the η - Cu_6Sn_5 . Reported benefits of having the η - Cu_6Sn_5 present in the interconnection are reduced thermal expansion, increased elastic modulus and hardness as well as improved creep properties [19, 21, 38, 40–42]. In addition, stresses related to polymorphic transformation due to volumetric difference of the hexagonal and monoclinic allotropies are avoided [38], which can inhibit cracking of the intermetallic compounds. In order to apply platinum as a contact metallization, it is highly important to examine the formation of the bonding microstructure and its evolution under annealing as well as possible interaction to Cu/Sn IMCs as the thermodynamic description of Cu–Pt–Sn ternary system is not available in the literature.

In this paper sputtered platinum is utilized as a contact metallization layer for electroplated Cu/Sn metallization. An adhesion layer for Pt was selected to be titanium in this study, as it is commonly used in the CMOS/MEMS industry [13]. In addition, the Cu/Sn stack is also soldered to bulk platinum (unlimited Pt available) in order to study the thermodynamic equilibria of the Cu–Pt–Sn system. These results are compared to the thin film platinum samples focusing on the microstructural evolution under a high temperature storage (HTS) test. As there is no Cu–Pt–Sn ternary system description available in the literature, the calculation of phase diagrams using the CALPHAD method was utilized to provide preliminary isothermal and vertical sections.

2 Materials and methods

A 40 nm thick TiW adhesion layer and a 500 nm thick gold seed layer were sputtered on thermally oxidized (300 nm SiO_2) silicon wafer. 5 μm of copper was electroplated utilizing NB Semiplat Cu 100 bath, followed by 7 μm of electroplated tin using NB Semiplat Sn 100 solution from NB technologies. Platinum was utilized as a contact metallization two ways: (1) as a sputtered layer on top of a 40 nm thick Ti adhesion layer on thermally oxidized silicon wafers

simulating realistic wafer-level metallization for bonding and (2) as a 100 μm thick bulk film (99.99% Goodfellow Inc) in order to study the reactions between the copper-tin metal stack and platinum. Both Cu/Sn and Ti/Pt metallized wafers were diced to 5 \times 5 mm pieces. The samples were soldered in air muffle furnace at 320 $^\circ\text{C}$ for 100, 500 and 2500 s by utilizing flux (Weller T0051383199), and air cooled to room temperature. The bonding procedures regarding time and temperature were selected to mimic wafer-level bonding conditions utilized for Au–Sn and Cu–Sn bonds [4, 5, 8, 10, 43–48]. The high temperature storage (HTS) aging test at 150 $^\circ\text{C}$ was conducted with a Heraeus Instruments oven for 500 and 1000 h. For the microstructural analysis, samples were cross-sectioned with standard metallographic methods. JEOL JSM-6330F field emission scanning electron microscope (SEM) with back-scattered electrons detector (BSE) and Oxford Instruments INCA X-sight energy-dispersive X-ray spectroscopy (EDX) equipment were used for the detailed microstructural analysis. The composition of phases was determined by averaging measurements from a minimum of five different locations with EDX (Fig. 1).

An electron-transparent lamella from the top die side (i.e. 1 μm from initial Cu/Sn interface) was prepared using an in-situ lift-out process with the using the dual-beam (SEM-FIB) FEI Helios NanoLab 600. Scanning transmission electron microscopy (STEM) micrographs, select area diffraction patterns (SADP) and EDX maps were collected using the JEOL-2800 transmission electron microscope (TEM) operated at 200 kV. The elemental mapping was made with a JEOL ultrafast silicon drift detector (SDD) with a large solid collection angle and a detection area of 100 mm^2 .

2.1 Thermodynamic modeling

In order to compose the thermodynamic description of the Cu–Pt–Sn system in this work, binary parameters were directly taken from the only thermodynamic description of Cu–Pt [49], and the latest updated assessments of Cu–Sn [50] and Pt–Sn [51]. Therefore, most of the original references evaluated in [50, 51] are not duplicated here.

The lattice stability of the element i ($i = \text{Cu}$, Pt and Sn), referred to the enthalpy of its stable state at 298.15 K and

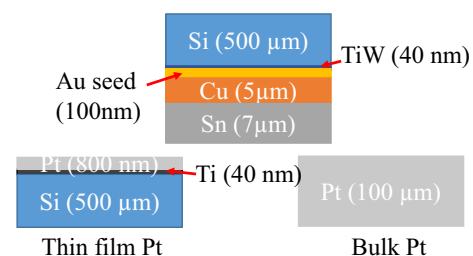


Fig. 1 Schematic presentation of samples

1 bar, H_i^{SER} , is recommended by Scientific Group Thermo-data Europe (SGTE) [52]. For details of analytical expressions of Gibbs energies and thermodynamic models of phases in binary systems, the reader may refer to descriptions in [49–51], here only the phase described in this work is briefly presented.

In order to include the effect of dissolved platinum, both η -Cu₆Sn₅ and PtSn phases have the prototype of NiAs structure [50, 51]. For the η -Cu₆Sn₅ phase, it was reported that the Wyckoff positions 2a and 2c were occupied by 100%Cu and 100%Sn, and the excess Cu atoms would occupy the 2d site [53]. In the PtSn crystal structure, the Pt and Sn atoms occupied the 2a and 2c sites respectively [54]. Consequently, the two phases were described with the (Cu, Pt)₁:(Cu, Va)₁:Sn₁ model, as was recommended for other NiAs or Ni₂In prototype phases by Kroupa [55]. The molar Gibbs energy was expressed by following equation.

$$G^{(Cu,Pt)_1:(Cu,Va)_1:Sn_1} = \sum_a \sum_b Y_a^I Y_b^{II} G_{a:b:Sn}^{(Cu,Pt)_1:(Cu,Va)_1:Sn_1} + RT(Y_{Cu}^I * \ln Y_{Cu}^I + Y_{Pt}^I * \ln Y_{Pt}^I) + RT(Y_{Cu}^{II} * \ln Y_{Cu}^{II} + Y_{Va}^{II} * \ln Y_{Va}^{II}) + Y_{Cu}^I Y_{Cu}^{II} Y_{Va}^{II} \left(\sum_{j=0,1}^j L_{Cu:(Cu,Va):Sn}^{(Cu,Pt)_1:(Cu,Va)_1:Sn_1} (Y_{Cu} - Y_{Va})^j \right) + Y_{Cu}^I Y_{Pt}^I Y_{Cu}^{II} \left(\sum_{j=0,1}^j L_{(Cu,Pt):Cu:Sn}^{(Cu,Pt)_1:(Cu,Va)_1:Sn_1} (Y_{Cu} - Y_{Pt})^j \right) \quad (1)$$

In Eq. (1), ‘a’ and ‘b’ refer to elements in the first and second sublattice sites, respectively. The Y terms are the site fractions of each constituent on relevant sublattice. R is the ideal gas constant and T is the temperature (in Kelvin). The L terms are the interaction energies between components on one sublattice (separated by a comma) when other sublattices are completely occupied by one of their components (separated by a colon). The binary parameters related to Cu–Sn and Pt–Sn were cited from the literature [50, 51], and the rest were evaluated in the present assessment to reproduce the solubility of Pt in η -Cu₆Sn₅ phase at 320 and 150 °C.

3 Results and discussion

During the bonding processes, both Cu and Pt dissolves into liquid tin and formed IMCs to the Cu/Sn and Pt/Sn interfaces. As can be seen from Figs. 2a, b and 3a, b, at the copper side of the bond, both Cu₆Sn₅ and Cu₃Sn phases were observed after soldering, and layer thicknesses were proportional to the soldering time (see Table 1). Platinum was detected in the Cu₆Sn₅ phase within all sample groups. Based on the SEM-EDX analysis (see Table 1), after 100 s

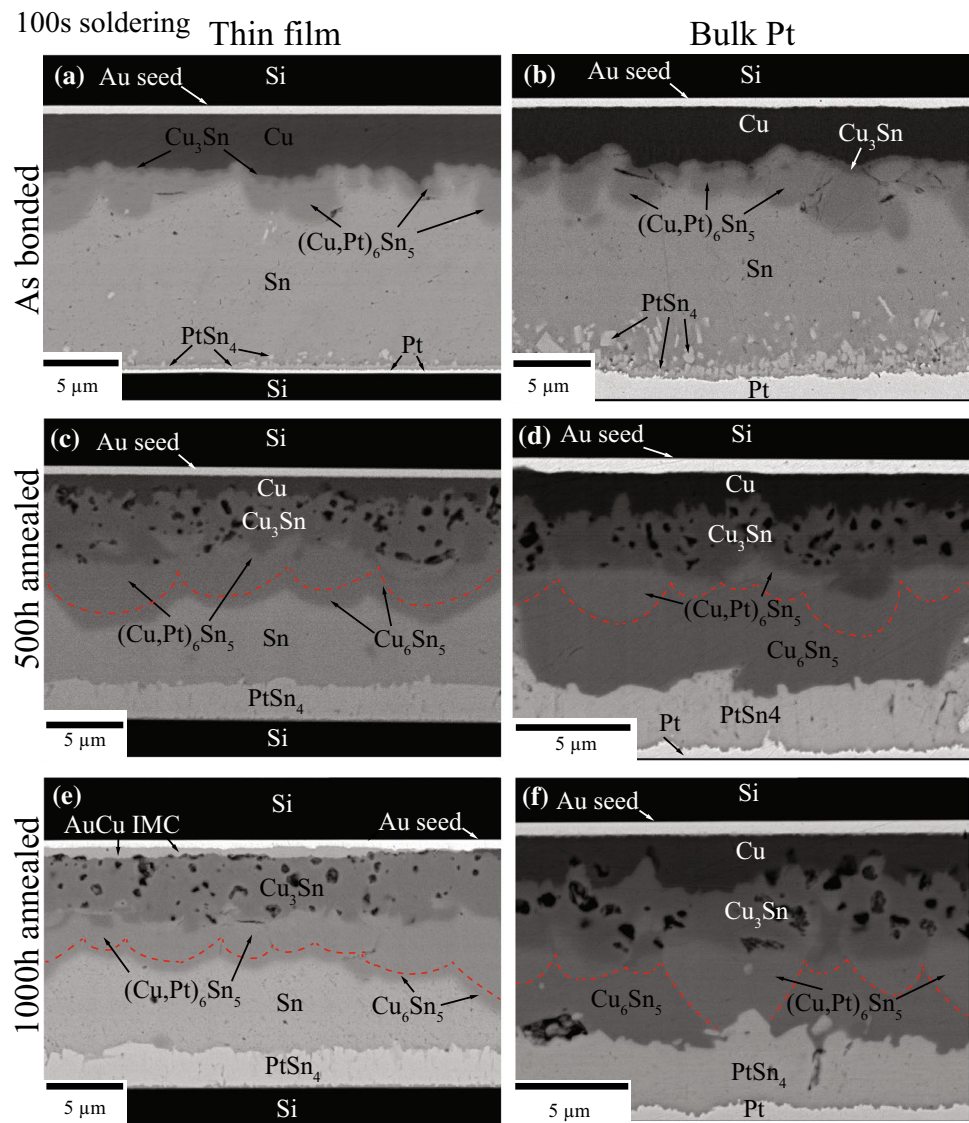
of soldering, the platinum content in the Cu₆Sn₅ phase was ~2 at%; and with 500 s reflow time ~3 at%, correspondingly. Thus, this phase was interpreted as (Cu, Pt)₆Sn₅. Thin film samples reflowed for 2500 s exhibited a microstructure consisting of mainly the (Cu, Pt)₆Sn₅ phase (see Fig. 4a), which had platinum solubility of ~5 at%. Platinum was not detected in the Cu₃Sn phase in any of the samples. However, in the Cu₃Sn phase, voiding was observed, which arises from the combination of electroplating process and chemistry utilized as well as Kirkendall effect [7, 56–61]. The 2500 s bulk platinum samples failed, as reactions had continued to the extent that copper had reacted completely and gold seed layer had started to participate to reactions. Thus, the samples were excluded from the further analysis.

As shown in Figs. 2a, b and 3a, b, platinum reacted with the tin during soldering, and formed the PtSn₄ phase within both thin film and bulk Pt samples. The PtSn₄ phase was thicker with bulk platinum samples, and some spalling of the PtSn₄ grains was observed into the tin during soldering. The amount of copper in the PtSn₄ phase was < 1 at% based on the EDX analysis i.e. below the detection limit of the equipment. Within the thin film samples, remaining thin layer of pure platinum was still observed after 100 and 500 s soldering times. The situation after 2500 s soldering time differed drastically compared to shorter reflow times: the platinum was completely consumed in thin film samples, and large PtSn₄ grains were observed in local equilibrium with Cu–Sn IMCs, as presented in Fig. 4a. In addition, the titanium adhesion layer had reacted with tin and dissolved copper, and formed small separate grains at the substrate interface.

The thickness of the (Cu, Pt)₆Sn₅ phase did not change significantly during annealing. Instead, an additional Cu₆Sn₅ phase layer grew on top of the original (Cu, Pt)₆Sn₅ grains that were formed in the reflow as shown in Figs. 2c–f and 3c–f. The interface between these two phases is highlighted with red dashed lines and a minor contrast difference in back-scatter electron images between these two phases can be perceived. Platinum was not detected with the SEM-EDX in this Cu₆Sn₅ phase. Meanwhile, the Cu₃Sn phase grew thicker within all sample groups, however, growth rate differed between thin film and bulk samples. In bulk samples, surplus of platinum atoms for the Pt–Sn reactions was assumed to decrease Sn diffusion towards copper, and thus, the Cu₃Sn layer was assumed to be thinner.

During annealing, the platinum continued reacting with the tin and the PtSn₄ phase grew thicker. The sputtered Pt layer was consumed completely during the first 500 h of annealing in all thin film samples. Other Pt–Sn IMCs were not detected in any of the samples even after 1000 h annealing, which is in line with the results presented by Yang et al. [12]. Platinum was not detected in the tin after annealing, and the copper solubility into Sn was at the detection limits of EDX (~1 at%).

Fig. 2 On the left column, the thin film Pt substrate samples and on the right column, the bulk Pt substrate samples with 100 s soldering time. **a** and **b** show the as bonded microstructure; **c** and **d** after 500 h annealing at 150 °C and **e** and **f** after 1000 h annealing at 150 °C. Red dashed line separates the $(\text{Cu, Pt})_6\text{Sn}_5$ and Cu_6Sn_5 phases. (Color figure online)



These observations correlate well with the thermodynamic description of the Pt–Sn and Cu–Sn systems [50, 51]. Reactions on the platinum side, i.e. formation of the PtSn_4 phase, is similar what has been reported in the literature both in soldering and under annealing [12, 18, 62]. As there was excess of platinum in the bulk substrate samples, the PtSn_4 layer was thicker (and respectively, the tin was consumed more) both after soldering and annealing. As platinum was found to dissolve into the $(\text{Cu, Pt})_6\text{Sn}_5$ grains at the opposite Cu/Sn side and not into the Cu_6Sn_5 layer that formed during annealing, a STEM-EDX analyses were performed in order to study these phases more in detail.

3.1 STEM-EDX analyses of $(\text{Cu, Pt})_6\text{Sn}_5$ and Cu_6Sn_5 phases

To confirm the SEM-EDX findings, STEM-EDX analyses of the copper side were undertaken from 1000 h annealed sample that was originally soldered for 500 s. Figure 5 shows the results of these analyses, and illustrates clearly two distinct Cu_6Sn_5 grain compositions. The $(\text{Cu, Pt})_6\text{Sn}_5$ grains located next the Cu_3Sn appear to have a significantly higher concentration of Pt when compared to the Cu_6Sn_5 layer formed during annealing.

To understand the difference between the dissimilar Cu_6Sn_5 grains, a select area diffraction pattern (SADP) analysis and diffraction simulation was undertaken in order to study the crystal structures. The results of the SADP indexing can be seen from Fig. 6. SADP at three zone-axes (ZA) were taken from both the Pt-rich and Pt-absent Cu_6Sn_5

Table 1 Compositions of the observed phases based on SEM-EDX analysis

IMC	Composition (at%)		Thickness (100 s soldering time)		Thickness (500 s soldering time)	
	As bonded	1000 h HTS	As bonded	1000 h HTS	As bonded	1000 h HTS
PtSn ₄	Cu: <1	Cu: <1	TF	TF	TF	TF
	Pt: <18	Pt: 18	0.4±0.1	2.2±0.2	0.7±0.3	2.3±0.2
	Sn: 81	Sn: 82	Bulk	Bulk	Bulk	Bulk
(Cu, Pt) ₆ Sn ₅	100 s	100 s	1.0±0.4	2.7±0.5	1.4±0.7	2.4±0.7
	Cu: 51 Pt: 2	Cu: 51 Pt: 2	TF	TF	TF	TF
	Sn: 47	Sn: 47	2.0±1.1	2.1±0.8	3.3±1.7	3.6±0.8
	500 s	500 s	Bulk	Bulk	Bulk	Bulk
	Cu: 50 Pt: 3	Cu: 51 Pt: 2	1.7±0.6	2.2±0.6	3.6±1.5	3.8±1.6
	Sn: 47	Sn: 47				
Cu ₆ Sn ₅	2500 s	2500 s				
	Cu: 50 Pt: 5	Cu: 48 Pt: 4				
	Sn: 45	Sn: 48				
Cu ₆ Sn ₅	–	Cu: 52 Pt: 0	–	TF	–	TF
		Sn: 48		1.0±0.1		1.3±0.5
				Bulk		Bulk
Cu ₃ Sn				1.2±0.7		0.4±0.2
	Cu: 75 Pt: 0	Cu: 75 Pt: 0	TF	TF	TF	TF
	Sn: 25	Sn: 25	0.3±0.1	3.7±0.5	0.6±0.1	3.9±0.5
			Bulk	Bulk	Bulk	Bulk
			0.5±0.2	1.7±0.5	0.6±0.2	1.9±0.5

grains. Each ZA contains a common reflection identified along the Kikuchi lines during imaging. In addition, the lamella tilt angles for each ZA were recorded. The diffraction simulation correlated the three lamella tilt angles, reflections and reflection angles to match the correct ZA. Results from the diffraction simulation and SADP fitting showed that the grains containing Pt were hexagonal η -Cu₆Sn₅, whereas the grains without Pt were the standard low temperature monoclinic η' -Cu₆Sn₅. It appears that the Pt stabilises the high temperature hexagonal form of the Cu₆Sn₅ at room temperature.

Based on the microstructural and STEM-EDX analyses at Cu/Sn interface, a following phase formation sequence regarding η and η' phases can be concluded. First, when tin melts, both copper and platinum dissolve rapidly into liquid. Second, after supersaturation of the liquid tin near the original interface, the heterogeneous nucleation occurs and platinum exhibits cross-interaction to IMC formation at the Cu/Sn interface (i.e. formation of η -(Cu, Pt)₆Sn₅). Third, these grains grow due to ripening flux mechanism and to the detriment of consumption of smaller grains. Last, under annealing, the platinum diffusion through solid tin is significantly slower (in practice insignificant as Pt is reacting with the tin and forms PtSn₄), and does not participate into formation of monoclinic Cu₆Sn₅. Meanwhile, copper diffuses both through the η -(Cu,Pt)₆Sn₅ formed during soldering, and especially through the grain boundaries. Due to the higher flux rate through grain boundaries, the η' -Cu₆Sn₅ forms first between and then on top of (Cu, Pt)₆Sn₅ grains, which can be

seen in Figs. 2c–f and 3c–f. In the next section, it is shown with thermodynamic analysis that hexagonal (Cu, Pt)₆Sn₅ is not in thermodynamic equilibrium with β -tin at 150 °C, and monoclinic η' -Cu₆Sn₅ should form in between.

3.2 The effect of platinum to the crystal structure of the Cu₆Sn₅ phase

As was shown, the platinum dissolves into the Cu₆Sn₅ phase, exhibiting similar phenomenon as Ni, Sb, Au, In and Zn [21, 27, 38, 39, 63–66], and based on the STEM analysis, stabilises the high temperature hexagonal (η) crystal structure. Previously Amagai [19] reported that alloying Sn with Pt nanoparticles and reflowing it on a copper substrate results Cu₆Sn₅ with 3.8 wt% solubility of Pt. Meanwhile, Wang et al. [18] did not detect any platinum in the Cu₆Sn₅ phase when Cu/Sn/Pt stack was reflowed even with extended durations. However, they had a thicker tin layer (150 μ m) between copper and platinum sheets, which can explain the difference in results. The hexagonal (η)—monoclinic (η') change has been previously determined to occur at 186 °C [27, 66, 67], but recent studies have shown that this transition temperature is in a range between 180 and 220 °C [21, 38, 63, 64]. On the other hand, as low as 1 at% of Ni in the Cu₆Sn₅ phase is sufficient to stabilize the high temperature hexagonal crystal form [21, 38, 39, 63, 64] to low temperatures, and even pure Cu₆Sn₅ can remain in hexagonal form depending on the cooling rate as kinetic requisites for the transformation are limited [27, 37, 38, 64, 66]. Nickel and

Fig. 3 On the left column, the thin film Pt substrate samples and on the right column, the bulk Pt substrate samples with 500 s soldering time. **a** and **b** show the as bonded microstructure; **c** and **d** after 500 h annealing at 150 °C and **e** and **f** after 1000 h annealing at 150 °C. Red dashed line separates the (Cu, Pt)₆Sn₅ and Cu₆Sn₅ phases. (Color figure online)

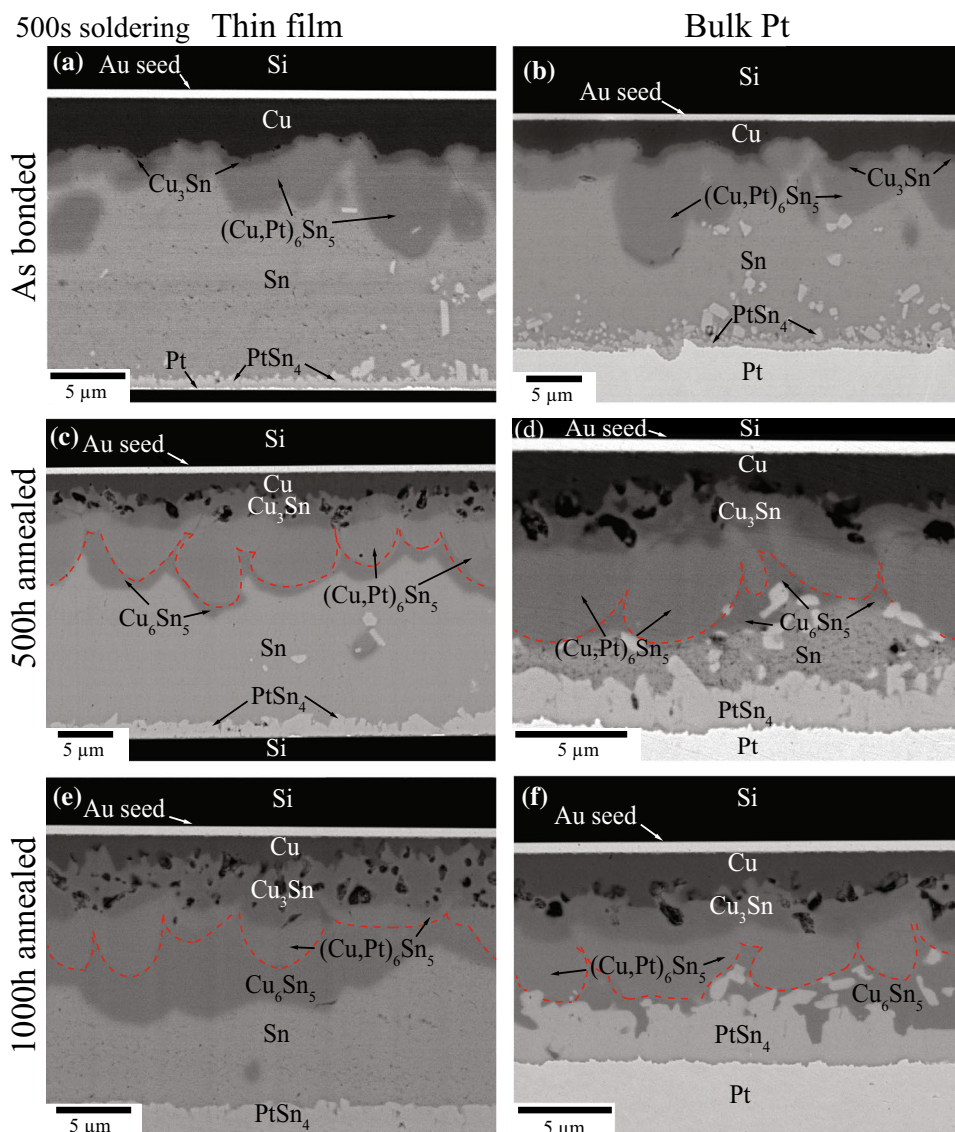
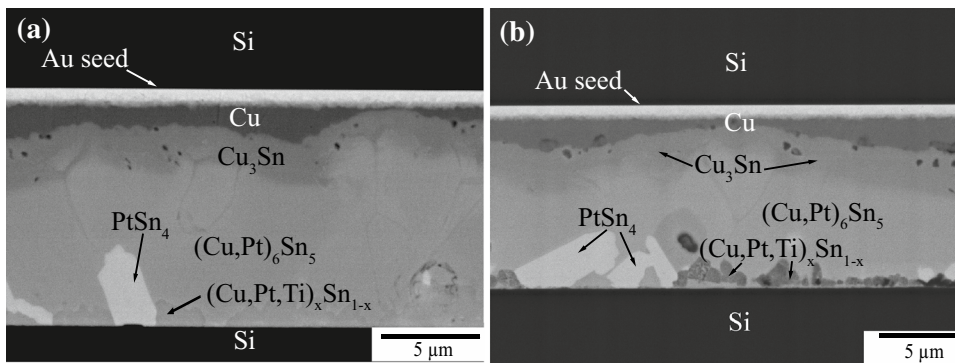


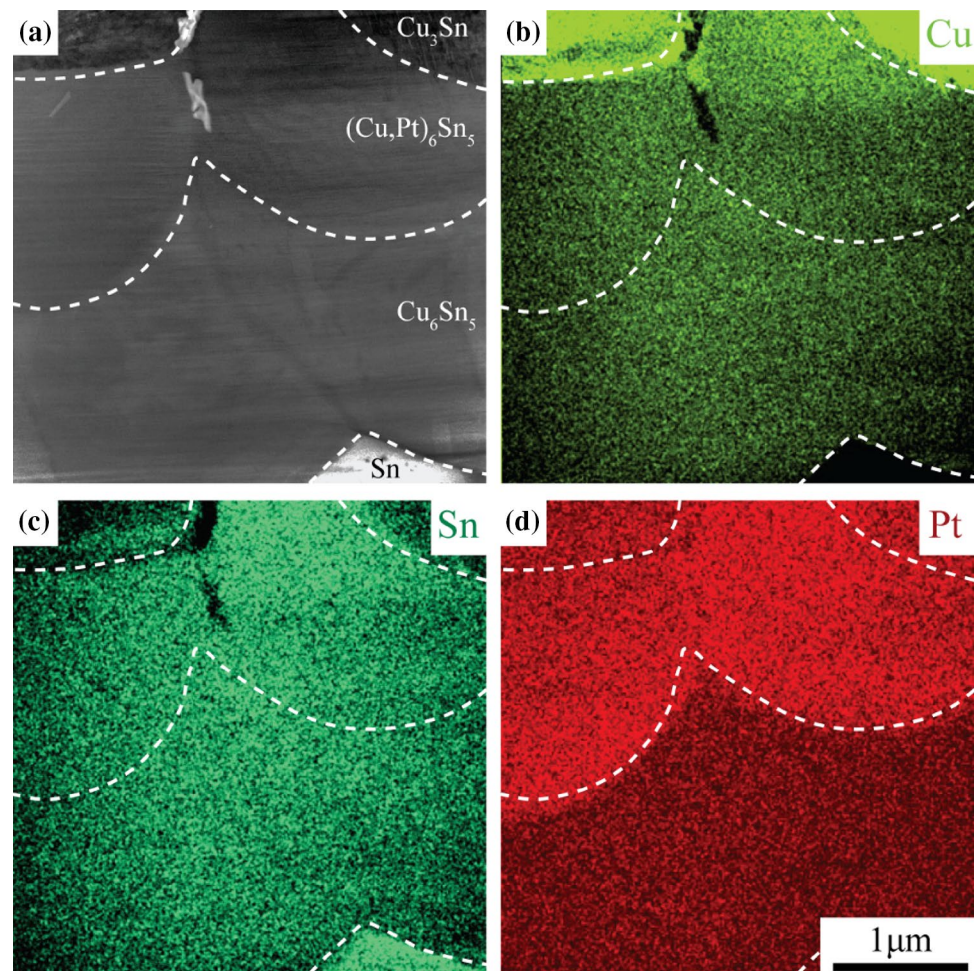
Fig. 4 2500 s soldered thin film samples **a** as bonded and **b** 1000 h annealed



gold [20, 23, 39] are known to replace copper atoms in the η-Cu₆Sn₅ unit cell, while Zn and In are substitutes for Sn [20, 38]. The stabilization effect of nickel has been more pronounced, probably due to difference in atom size when

compared to Au, and thus, the induced stress to surrounding atoms is different [22, 25, 67]. Several time-temperature-transformation (TTT) curves of the hexagonal to monoclinic transformation have been reported, and highlighted

Fig. 5 STEM-EDX analysis of Pt rich $(\text{Cu, Pt})_6\text{Sn}_5$ grains with the boundaries between Pt-rich and Pt-absent Cu_6Sn_5 grains indicated with dashed lines, **a** BF micrograph, -EDX maps of **b** Cu, **c** Sn and **d** Pt



that factors such as cooling rate from bonding temperature and possible solid-state high temperature annealing have significant impact on the kinetics [15, 19, 21, 22, 24]–[26].

In order to study the effect of platinum in the Cu_6Sn_5 phase more in detail, the preliminary thermodynamic analysis was performed for the Cu–Pt–Sn system. The descriptions of these three binary systems were combined and the models for the observed phases were adapted in order to describe the detected solubility of the third element especially in the hexagonal $\eta\text{-Cu}_6\text{Sn}_5$. The parameters used to describe the solubility of the Pt element in the $\eta\text{-Cu}_6\text{Sn}_5$ and $\eta'\text{-Cu}_6\text{Sn}_5$ phases, were adjusted by progressively taking into account the experimentally determined phase equilibria and composition ranges. At each step of the evaluation, a systematic comparison has been done between all available experimental results and the calculated one. The evaluated thermodynamic parameters obtained in the present work are listed in Table 2.

Isothermal sections optimized based on the experimental data determined in this work at 150 °C as well as at 320 °C are presented in Fig. 7. In Fig. 7a, the complete isothermal section at 150 °C is presented. In order to visualize the

phase equilibria observed in the microstructures, enlargement from Sn rich corner at 320 and 150 °C is presented in Fig. 7b, c, respectively. A schematic presentation from the Cu_6Sn_5 region is in Fig. 7d, where one can observe that $\eta\text{-(Cu, Pt)}_6\text{Sn}_5$ phase in equilibria with Cu_3Sn , $\eta'\text{-Cu}_6\text{Sn}_5$ and PtSn_4 phases. Thus, isothermal section at 150 °C explains the monoclinic $\eta'\text{-Cu}_6\text{Sn}_5$ phase formation in between the $\beta\text{-Sn}$ and $\eta\text{-(Cu, Pt)}_6\text{Sn}_5$ phases under annealing at 150 °C, as $\eta'\text{-Cu}_6\text{Sn}_5$ is in equilibria with $\eta\text{-(Cu, Pt)}_6\text{Sn}_5$, $\beta\text{-Sn}$ and PtSn_4 . On the other hand, as shown in Fig. 7b, reactions and phase sequence observed after bonding can be reasoned as the hexagonal $(\text{Cu, Pt})_6\text{Sn}_5$ is in equilibrium with Cu_3Sn , $\beta\text{-Sn}$ and PtSn_4 phases at soldering temperature of 320 °C.

In order to explain the effect of dissolved platinum into the Cu_6Sn_5 phase, a vertical section from Cu_6Sn_5 with constant Sn concentration of 45 at% along the purple line superimposed in Fig. 7, is presented in Fig. 8. As can be seen from this figure, the dissolved Pt decreases strongly the $\eta \Rightarrow \eta'$ transition temperature (see purple arrow in Fig. 8.). Thermodynamic analysis indicates that $(\text{Cu, Pt})_6\text{Sn}_5$ should transform to monoclinic crystal structure at ~ 120 °C, which was not observed in the STEM analysis (performed ~ 1 month

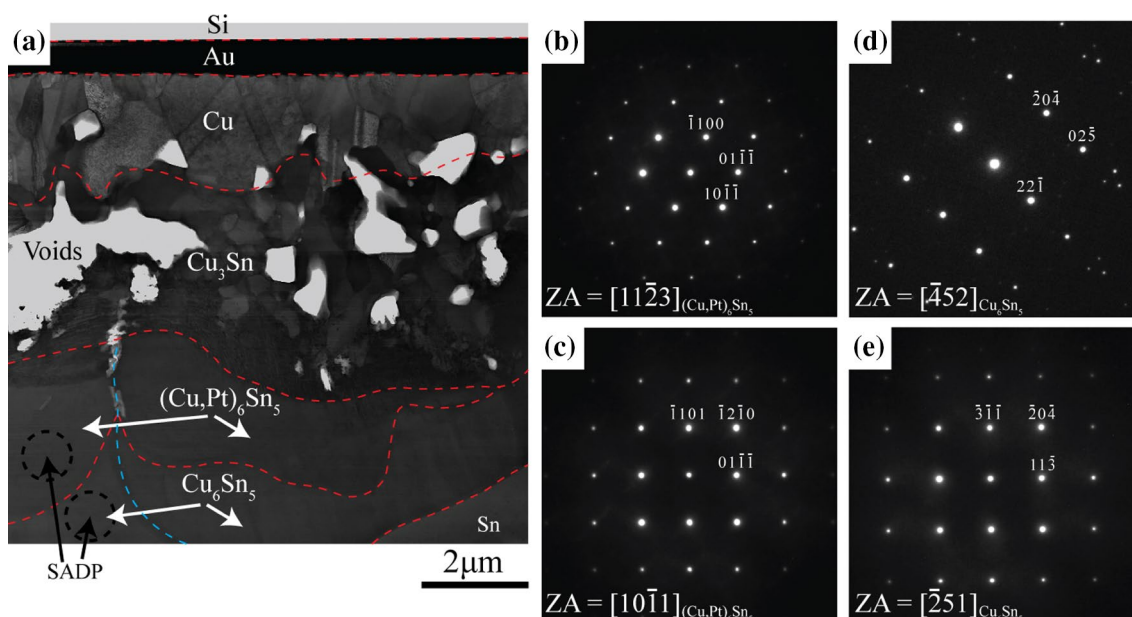


Fig. 6 SADP analysis of the crystal structure of the Pt-rich and Pt-absent Cu_6Sn_5 grains. Subfigure **a** is a STEM-BF micrograph of the Cu bonded side, with the SADP regions indicated and the phase boundaries highlighted by the red dashed line and the blue dashed

line separating the η - $(\text{Cu,Pt})_6\text{Sn}_5$ and Cu_6Sn_5 grains. Sub figures **b**, **c** are the SADP of the hexagonal η - $(\text{Cu,Pt})_6\text{Sn}_5$ grain and **d–e** are the SADP of the monoclinic η' - Cu_6Sn_5 grain from two zone-axes

Table 2 Thermodynamic parameters assessed in this work

Defined functions, and phases	Parameters obtained in this work
NiAs (representing η - Cu_6Sn_5 and PtSn): $(\text{Cu}, \text{Pt})_1:(\text{Cu}, \text{Va})_1:\text{Sn}_1$	$G_{\text{Pt:Pt:Sn}}^{\text{NiAs}} = +5000 + 2 * \text{GHSE RPT} + \text{GHSE RSN}$ $G_{\text{Pt:Cu:Sn}}^{\text{NiAs}} = +15000 + \text{GHSE RCU} + \text{GHSE RPT} + \text{GHSE RSN}$ $G_{\text{Cu:Pt:Sn}}^{\text{NiAs}} = +15000 + \text{GHSE RCU} + \text{GHSE RPT} + \text{GHSE RSN}$ ${}^0L_{(\text{Cu,Pt}): \text{Cu:Sn}}^{\text{NiAs}} = -100000$ ${}^1L_{(\text{Cu,Pt}): \text{Cu:Sn}}^{\text{NiAs}} = -80000$

Values are in SI units. Parameters of sub-binary systems of Cu–Pt–Sn were directly cited from the literature, i.e. Cu–Sn from [50], Cu–Pt from [49], and Pt–Sn from [51]. And data for pure elements are taken from SGTE [52]

after the end of the annealing). Similar effect even with pure Cu–Sn binary system is commonly detected, as the transform does not occur within a reasonable time because of kinetic constraints [20, 27, 38, 64, 66].

Generally, platinum appears to stabilize high temperature hexagonal (η) crystal structure of the Cu_6Sn_5 phase similar as nickel. To compare this stabilization effect of platinum and nickel, the graph of Gibbs free energy as function of composition of the third element (i.e. a G - x_i diagram) in the Cu_6Sn_5 phase was calculated and is presented in Fig. 9. A stronger stabilizing effect is obtained with platinum compared to nickel. Authors would like to highlight, that the solubility of the nickel in the Cu_6Sn_5 phase is larger [24, 26, 28, 38, 68] than now observed with platinum, and thus, the overall stabilization effect can be higher with Ni than Pt. Meanwhile, it is plausible to assume that, as the crystal

transformation $\eta' \rightarrow \eta$ is sluggish in pure Cu–Sn system due to kinetics constrains, introducing a ternary element that further stabilizes the η' -phase (i.e. decreases the Gibbs free energy significantly), the transformation becomes even more obstructed. Thus, it is reasonable to observe both η - and η' -phases even after annealing. On the other hand, η to η' transformation may induce local stresses due to 2.15% volumetric expansion (pure Cu_6Sn_5 without third elements) [22, 32, 38, 40, 42, 67]. Therefore, stabilization of the high temperature hexagonal crystal structure can enhance the reliability of the joints by preventing the IMC cracking [27, 38, 39, 64, 66, 69]. Hence, platinum provides to be a potential candidate as a contact metallization for Cu–Sn interconnections exhibiting similar characteristics as nickel in stabilizing the hexagonal crystal structure of the Cu_6Sn_5 phase.

Fig. 7 The calculated isothermal section of Cu–Pt–Sn at **a** 150 °C and **b** 320 °C, experimental data were superimposed on. **c** Partial isothermal section at 150 °C showing the Sn rich part of the isothermal section in **(a)**. **d** High magnification from the region around the Cu_6Sn_5 phase demonstrating the phase equilibria. Superimposed purple line indicates the direction of vertical section and Gibbs energy diagram shown in Fig. 8 and 9

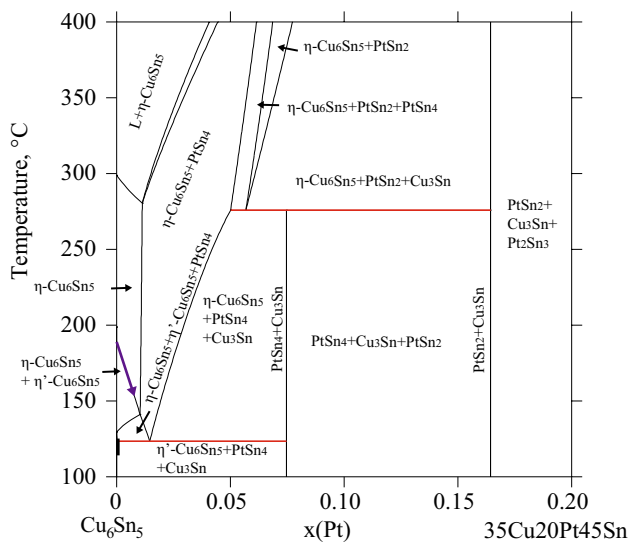
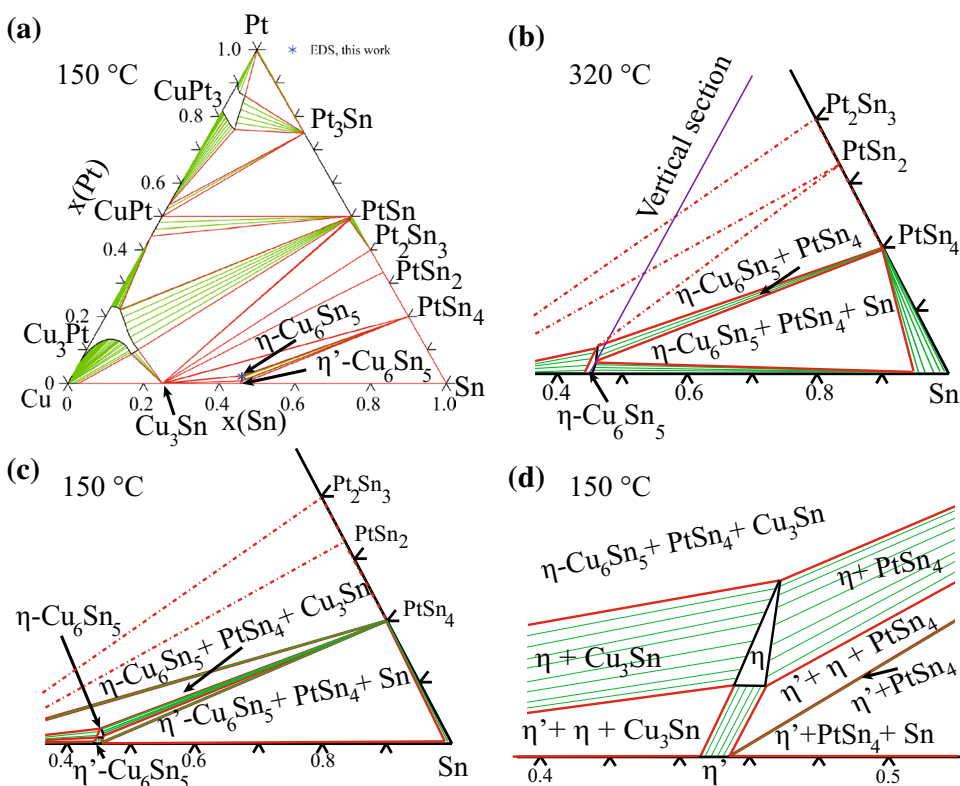


Fig. 8 Partial vertical section along the dashed line shown in Fig. 8 from pure Cu_6Sn_5 towards hypothetical Pt_6Sn_5 i.e. constant Sn content

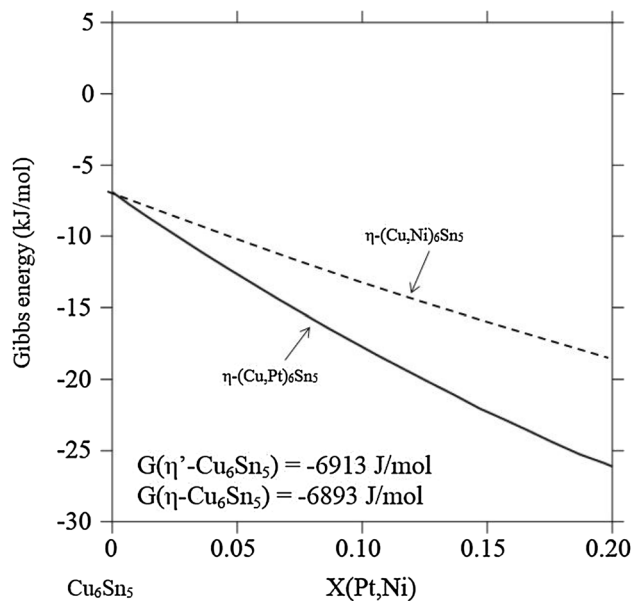


Fig. 9 Gibbs energy diagram of the $(\text{Cu}, \text{Pt})_6\text{Sn}_5$ at 150 °C as a function of Pt (solid line) content through the vertical section shown in Fig. 9. The effect of dissolved Ni (dashed line) in $(\text{Cu}, \text{Ni})_6\text{Sn}_5$ is superimposed based on the data from [68]

4 Conclusions

Viability of platinum as a contact metallization for Cu/Sn bonding metallization was studied in this paper. Platinum was observed to dissolve into the Cu_6Sn_5 phase formed at the Cu-Sn interface during soldering process and form $(\text{Cu}, \text{Pt})_6\text{Sn}_5$ intermetallic compound. In addition, platinum was discovered to stabilize the high temperature hexagonal (η) crystal structure of the $(\text{Cu}, \text{Pt})_6\text{Sn}_5$ phase to room temperature, and polymorphic transformation to low temperature monoclinic crystal structure was not observed even after 1000 h high temperature storage test at 150 °C. On the other hand, platinum was not observed to dissolve into the Cu_6Sn_5 phase having the monoclinic crystal structure, which grows between the $(\text{Cu}, \text{Pt})_6\text{Sn}_5$ grains and Sn during annealing. Meanwhile, copper was not observed to dissolve into the PtSn_4 phase formed at platinum metallization interface. Thermodynamic analysis was performed and isothermal section, vertical section and Gibbs energy diagram were presented. The stabilizing effect of platinum in the hexagonal Cu_6Sn_5 was discovered to be even more pronounced than in the case of nickel that has been investigated extensively in the literature. Due to the fact that IMCs in the high density interconnections are large fraction of the bump, it is highly important to understand the microstructure after bonding as well as reactions taking place under operation. Altogether, platinum is a potential contact metallization for 3D-integration of electronics and sensors, where only limited selection of elements can be utilized in e.g. biomedical applications, MEMS or IC-wafer processing.

Acknowledgements This work has been carried out as a part of an Eniac Project Lab4MEMS II (Grant Number 2013-2-621176). The authors would like to acknowledge the Innovation Funding Agency Business Finland (formerly Tekes), Okmetic and Murata Electronics for financial support. The authors acknowledge the provision of facilities as well as technical support by Aalto University at OtaNano—Nanomicroscopy Center (Aalto-NMC).

References

- W. Arden, M. Brillouët, P. Coge, M. Graef, B. Huizing, R. Mahnkopf, J. Pelka, J. Pfeiffer, A. Rouzaud, M. Tartagni, C. Van Hoof, J. Wagner, Towards a More-than-Moore roadmap, CATRENE Scientific Committee (2011)
- A. Heinig, M. Dietrich, A. Herkersdorf, F. Miller, T. Wild, K. Hahn, A. Grunewald, R. Bruck, S. Krohnert, J. Reisinger, in *Design, Automation and Test in Europe Conference and Exhibition (DATE), 2014* (IEEE, 2014), pp. 1–9
- A. Hilton, D.S. Temple, *Sensors Rev.* **16**, 1819 (2016)
- M. Tilli, T. Motooka, S. Franssila, M. Paulasto-Krockel, V.-M. Airaksinen, V. Lindroos, *Handbook of Silicon Based MEMS Materials and Technologies*, 2nd edn. (Elsevier, Amsterdam, 2015)
- P. Ramm, J. Ji.-Q. Lu, M.M.V. Taklo, *Handbook of Wafer Bonding* (Wiley, New York, 2012)
- H.Y. Chuang, T.L. Yang, M.S. Kuo, Y.J. Chen, J.J. Yu, C.C. Li, C.R. Kao, *IEEE Trans. Device Mater. Reliab.* **12**, 233 (2012)
- Y. Wang, S.H. Chae, J. Im, P.S. Ho, in *Electronic Components and Technology Conference (ECTC), 2013 IEEE 63rd* (IEEE, 2013), pp. 1953–1958
- H. Liu, G. Salomonsen, K. Wang, K.E. Aasmundtveit, N. Hoivik, *IEEE Trans. Components, Packag. Manuf. Technol.* **1**, 1350 (2011)
- T.T. Luu, A. Duan, K.E. Aasmundtveit, N. Hoivik, *J. Electron. Mater.* **42**, 3582 (2013)
- A. Rautiainen, H. Xu, E. Österlund, J. Li, V. Vuorinen, M. Paulasto-Kröckel, *J. Electron. Mater.* **44**, 4533 (2015)
- A. Duan, K. Wang, K.E. Aasmundtveit, N. Hoivik, in *Electronic System-Integration Technology Conference (ESTC), 2012 4th* (IEEE, 2012), pp. 1–5
- S.C. Yang, W.C. Chang, Y.W. Wang, C.R. Kao, *J. Electron. Mater.* **38**, 25 (2009)
- J. Kuhmann, C.-H. Chiang, P. Harde, F. Reier, W. Oesterle, I. Urban, A. Klein, *Mater. Sci. Eng. A* **242**, 22 (1998)
- H. Tang, F. Yan, Q. Tai, H.L.W. Chan, *Biosens. Bioelectron.* **25**, 1646 (2010)
- P.J. Yang, V.V. Halbach, R.T. Higashida, G.B. Hieshima, *Am. J. Neuroradiol.* **9**, 547 (1988)
- N. Lago, K. Yoshida, K.P. Koch, X. Navarro, *IEEE Trans. Biomed. Eng.* **54**, 281 (2007)
- A. Cowley, B. Woodward, *Platin. Met. Rev.* **55**, 98 (2011)
- S.J. Wang, C.Y. Liu, *Acta Mater.* **55**, 3327 (2007)
- M. Amagai, *Microelectron. Reliab.* **48**, 1 (2008)
- G. Zeng, S.D. McDonald, D. Mu, Y. Terada, H. Yasuda, Q. Gu, M.A.A.M. Salleh, K. Nogita, *J. Alloys Compd.* **685**, 471 (2016)
- K. Nogita, M.A.A. Mohd Salleh, E. Tanaka, G. Zeng, S.D. McDonald, S. Matsumura, *Jom* **68**, 2871 (2016)
- C. Yu, J. Liu, H. Lu, P. Li, J. Chen, *Intermetallics* **15**, 1471 (2007)
- K. Nogita, *Intermetallics* **18**, 145 (2010)
- K. Nogita, T. Nishimura, *Scr. Mater.* **59**, 191 (2008)
- K. Nogita, D. Mu, S.D. McDonald, J. Read, Y.Q. Wu, *Intermetallics* **26**, 78 (2012)
- J.Y. Tsai, Y.C. Hu, C.M. Tsai, C.R. Kao, *J. Electron. Mater.* **32**, 1203 (2003)
- T. Laurila, V. Vuorinen, M. Paulasto-Kröckel, *Mater. Sci. Eng. R* **68**, 1 (2010)
- T. Laurila, J. Hurtig, V. Vuorinen, J.K. Kivilahti, *Microelectron. Reliab.* **49**, 242 (2009)
- Y.W. Wang, Y.W. Lin, C.T. Tu, C.R. Kao, *J. Alloys Compd.* **478**, 121 (2009)
- F. Gao, T. Takemoto, H. Nishikawa, *Mater. Sci. Eng. A* **420**, 39 (2006)
- Y.W. Wang, C.C. Chang, C.R. Kao, *J. Alloys Compd.* **478**, 4 (2009)
- G. Zeng, S.D. McDonald, Q. Gu, S. Suenaga, Y. Zhang, J. Chen, K. Nogita, *Intermetallics* **43**, 85 (2013)
- I.E. Anderson, J.L. Harringa, *J. Electron. Mater.* **33**, 1485 (2004)
- I.E. Anderson, J.L. Harringa, *J. Electron. Mater.* **35**, 94 (2006)
- C.E. Ho, T.T. Kuo, C.C. Wang, W.H. Wu, *Electron. Mater. Lett.* **8**, 495 (2012)
- C.E. Ho, T.T. Kuo, W. Gierlotka, F.M. Ma, *J. Electron. Mater.* **41**, 3276 (2012)
- G. Zeng, S.D. McDonald, J.J. Read, Q. Gu, K. Nogita, *Acta Mater.* **69**, 135 (2014)
- D.K. Mu, S.D. McDonald, J. Read, H. Huang, K. Nogita, *Curr. Opin. Solid State Mater. Sci.* **20**, 55 (2016)
- Y.Q. Wu, S.D. McDonald, J. Read, H. Huang, K. Nogita, *Scr. Mater.* **68**, 595 (2013)
- D. Mu, H. Huang, K. Nogita, *Mater. Lett.* **86**, 46 (2012)

41. H. Tsukamoto, Z. Dong, H. Huang, T. Nishimura, K. Nogita, *Mater. Sci. Eng. B* **164**, 44 (2009)
42. D. Mu, H. Huang, S.D. McDonald, J. Read, K. Nogita, *Mater. Sci. Eng. A* **566**, 126 (2013)
43. V. Vuorinen, A. Rautiainen, M. Paulasto-Krockel, In *20th European Microelectronics and Packaging Conference and exhibition. Enabling technologies for a better life future, EMPC 2015* (2016)
44. V. Vuorinen, A. Rautiainen, H. Heikkinen, M. Paulasto-Kröckel, *Microelectron. Reliab.* **64**, 676–680 (2016)
45. A. Rautiainen, V. Vuorinen, H. Heikkinen, M. Paulasto-Krockel, *IEEE Trans. Components, Packag. Manuf. Technol.* **8**, 169–176(2018)
46. K.E. Aasmundtveit, K. Wang, N. Hoivik, J.M. Graff, A. Elfving, *Microelectronics and packaging conference 2009. EMPC 2009.* *Eur. J* (2009)
47. T.T. Luu, A. Duan, K. Wang, K.E. Aasmundtveit, N. Hoivik, 2012 4th Electronic system-integration technology conference (ESTC), pp 1–5 (2012)
48. H. Liu, G. Salomonsen, K. Wang, K.E. Aasmundtveit, N. Hoivik, *Test J*, 1 (2011)
49. T. Abe, B. Sundman, H. Onodera, *J. Phase Equilib. Diffus.* **27**, 5 (2006)
50. H.Q. Dong, V. Vuorinen, X.M. Tao, T. Laurila, M. Paulasto-Kröckel, *J. Alloys Compd.* **588**, 449 (2014)
51. V. Grolier, R. Schmid-Fetzer, *J. Alloys Compd.* **450**, 264 (2008)
52. A. Dinsdale, *SGTE Unary Database, Version 5.0* (n.d.)
53. G. Aurelio, S.A. Sommadossi, G.J. Cuello, *J. Electron. Mater.* **41**, 3223 (2012)
54. K.L. Shelton, P.A. Merewether, B.J. Skinner, *Can. Minerol.* **19**, 599 (1981)
55. A. Kroupa, *Comput. Mater. Sci.* **66**, 3 (2013)
56. G. Ross, H. Xu, V. Vuorinen, M. Paulasto-Krockel, *Proceedings of the 5th Electronics System-Integration Technology Conference, ESTC 2014*, 1 (2014)
57. G. Ross, V. Vuorinen, M. Paulasto-Kröckel, *Proceeding-electronic components and technology conference*, pp 2193–2199 (2015)
58. G. Ross, V. Vuorinen, M. Paulasto-Kröckel, *J. Alloys Compd.* **677**, 127 (2016)
59. F. Wafula, Y. Liu, L. Yin, P. Borgesen, E.J. Cotts, N. Dimitrov, *J. Appl. Electrochem.* **41**, 469 (2011)
60. Y. Liu, J. Wang, L. Yin, P. Kondos, C. Parks, P. Borgesen, D.W. Henderson, E.J. Cotts, N. Dimitrov, *J. Appl. Electrochem.* **38**, 1695 (2008)
61. L. Yin, P. Borgesen, *J. Mater. Res.* **26**, 455 (2011)
62. B. Meagher, D. Schwarcz, M. Ohring, *J. Mater. Sci.* **31**, 5479 (1996)
63. Y.Q. Wu, J.C. Barry, T. Yamamoto, Q.F. Gu, S.D. McDonald, S. Matsumura, H. Huang, K. Nogita, *Acta Mater.* **60**, 6581 (2012)
64. K. Nogita, C.M. Gourlay, S.D. McDonald, Y.Q. Wu, J. Read, Q.F. Gu, *Scr. Mater.* **65**, 922 (2011)
65. M.A.A. Mohd Salleh, S.D. McDonald, H. Yasuda, A. Sugiyama, K. Nogita, *Scr. Mater.* **100**, 17 (2015)
66. T. Laurila, V. Vuorinen, J.K. Kivilahti, *Mater. Sci. Eng. R* **49**, 1 (2005)
67. G. Ghosh, M. Asta, *J. Mater. Res.* **20**, 3102 (2011)
68. H. Yu, V. Vuorinen, J.K. Kivilahti, *J. Electron. Mater.* **36**, 136 (2007)
69. W.Y. Chen, W. Tu, H.C. Chang, T.T. Chou, J.G. Duh, *Mater. Lett.* **134**, 184 (2014)